Quantum perfect crossed Andreev reflection in top-gated quantum anomalous Hall insulator–superconductor junctions

Ying-Tao Zhang,[1] Zhe Hou,[2] X. C. Xie,[2,3] and Qing-Feng Sun[2,3,*]
[1]*College of Physics, Hebei Normal University, Shijiazhuang 050016, China*
[2]*International Center for Quantum Materials, School of Physics, Peking University, Beijing 100871, China*
[3]*Collaborative Innovation Center of Quantum Matter, Beijing 100871, China*
(Received 4 January 2017; revised manuscript received 11 June 2017; published 29 June 2017)

We investigate the quantum tunneling and Andreev reflection in a top-gated quantum anomalous Hall insulator proximity coupled with a superconductor junction. A quantized perfect crossed Andreev reflection with its coefficient being integer 1 is obtained and all other scattering processes (the normal reflection, normal tunneling, and local Andreev reflection) are completely suppressed when the topological superconductor phase with Chern number $\mathcal{N} = 1$ is realized. This perfect crossed Andreev reflection originates from the tunneling of the chiral Majorana edge states, and the phase of tunneling amplitude only being 0 and π plays a decisive role. Furthermore, because of the chiral characteristic of the Majorana edge states, the perfect crossed Andreev reflection is robust against the disorder and can work in a wide range of system parameters.

DOI: 10.1103/PhysRevB.95.245433

I. INTRODUCTION

With the expectation on the utilization of entanglement effects in quantum communication and computation, quantum entanglement has been an extremely active area attracting many researchers [1–3]. One of the most key issues is searching for the methods of creating entangled particles. A Cooper pair in the superconductor is a pair of electrons bound together in a certain manner, which are both spin and momentum entangled. Thus a superconductor is deemed as a natural source for generating nonlocal Einstein–Podolsky–Rosen electron pairs [4,5]. A Cooper pair can be spatially separated with the help of the crossed Andreev reflection (CAR) [6–10], a process of converting an incoming electron from one terminal into an outgoing hole at the other terminal. These spatially separated entangled electrons are the key building blocks for its promising application in quantum communication and quantum computing [11–17]. Therefore, many Cooper-pair splitters by coupling a superconductor with quantum dots [9,18–21], carbon nanotubes [22,23], Luttinger liquid wires [24], graphene [25–27], etc. [28], have been theoretically put forward and experimentally implemented in part.

However, besides the CAR, there also exists local Andreev reflection (LAR) [29], where the outgoing hole returns back to the same terminal as the incoming electron. Since the incoming electrons and outgoing holes in the LAR reside in the same terminals, the LAR is usually stronger than the CAR. Moreover, the CAR is often completely masked by another nonlocal process known as quantum tunneling, which does not involve Cooper pairs and is therefore a parasitic process [8,30]. In the experiment, impurities and disorders exist inevitably, which cause the normal reflection and weaken the CAR. Therefore, the coefficient of the CAR is usually very small. To obtain a perfect CAR with its coefficient being 1, it is necessary to propose a system where the LAR, normal tunneling, and the normal reflection are all completely suppressed and then all incident electrons are converted into holes in the other terminal.

A quantum anomalous Hall insulator (QAHI) is a special kind of material where quantum Hall effects can be realized in the absence of an external magnetic field, and the unidirectionality of the chiral edge states promises the absence of backscattering [31–35]. A QAHI in proximity to an s-wave superconductor can induce a topological superconductor (TSC) [36], which supports topologically protected chiral Majorana edge states [37,38]. In the past proposed system based on the QAHI proximity-coupled with a superconductor junction [39], it was found that the LAR could be completely suppressed and the CAR could be considerably improved. But the normal tunneling process exists, and the CAR is still not perfect.

In this paper, we investigate normal tunneling, the LAR, and the CAR in a top-gated QAHI proximity coupled with a superconductor, as shown in Fig. 1(a), in which the top-gated voltage can moderate the transition of TSC phase with Chern number from $\mathcal{N} = 2$ to $\mathcal{N} = 1$. We find that, in the TSC phase with $\mathcal{N} = 1$, a quantized perfect CAR occurs in which the CAR coefficient shows a plateau with its value being integer 1, and all other scattering processes, e.g., LAR, normal tunneling, and normal reflection, are completely suppressed. This perfect CAR originates from the tunneling of the chiral Majorana edge states, and the phase of the tunneling amplitude only being 0 and π plays a decisive role. Because of the chiral characteristic of the Majorana edge states, the perfect CAR is robust against the disorder and can survive over a wide range of system parameters.

The rest of the paper is organized as follows: In Sec. II, we present the model Hamiltonian of the QAHI-TSC-QAHI junction and show the formulas of the tunneling coefficient, the LAR coefficient, and the CAR coefficient. In Sec. III, we investigate the quantum perfect CAR effect. At last, the results are summarized in Sec. IV.

II. MODEL AND METHOD

For definiteness, we consider the simplest QAHI model Hamiltonian realized with low-energy states near the Γ point:

$$H_{\mathrm{QAHI}}(p) = \begin{pmatrix} m + Bp^2 + \mu_L & A(p_x - ip_y) \\ A(p_x + ip_y) & -m - Bp^2 + \mu_L \end{pmatrix}, \quad (1)$$

*sunqf@pku.edu.cn

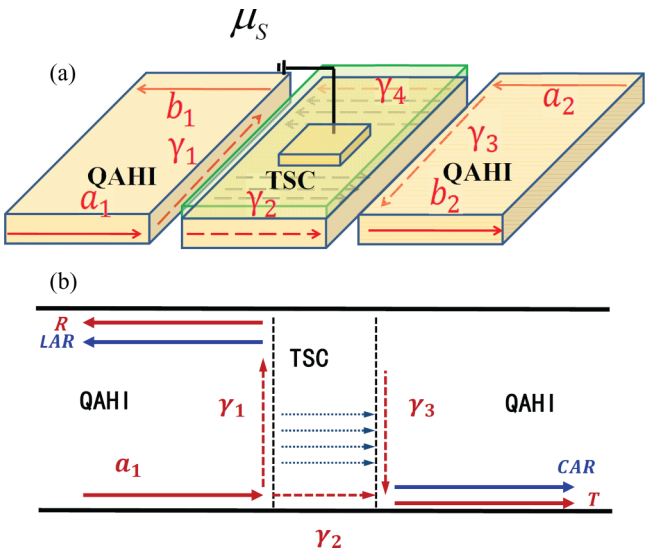

FIG. 1. (a) Schematic diagram of a QAHI-TSC-QAHI junction. Red solid and dotted arrows label the propagating direction of the chiral edge states and Majorana edge states. (b) Schematic diagram of the propagating route for an electron incoming from the left terminal to the QAHI-TSC-QAHI junction. Here the central TSC is at the $\mathcal{N} = 1$ phase. Red solid (dotted) arrows label the chiral electron (Majorana) edge states. The blue dotted arrows describe the tunneling from Majorana edge state γ_1 to γ_3.

where A, B, and m are material parameters, and μ_L is the potential energy of the QAHI leads. The basis vector is $(c_\uparrow(p),c_\downarrow(p))^T$, where $c_\uparrow(p)$ $[c_\downarrow(p)]$ is the operator annihilating an electron of momentum p and spin $\uparrow$ $(\downarrow)$. The sign of m/B determines the topological properties of the system, and the QAHI is obtained by setting $m/B < 0$. Since the tight-binding representation is used in our calculations, the Hamiltonian can be mapped onto a nearest-neighbor tight-binding representation on a two-dimensional square lattice,

$$\begin{aligned} H &= \sum_i [\psi_i^\dagger T_0 \psi_i + (\psi_i^\dagger T_x \psi_{i+\delta\hat{\mathbf{x}}} + \psi_i^\dagger T_y \psi_{i+\delta\hat{\mathbf{y}}}) + \text{H.c.}], \\ T_0 &= [m + (4B\hbar^2/a^2)]\sigma_z + \mu_L \sigma_0, \\ T_x &= -(B\hbar^2/a^2)\sigma_z - (iA\hbar/2a)\sigma_x, \\ T_y &= -(B\hbar^2/a^2)\sigma_z - (iA\hbar/2a)\sigma_y, \end{aligned} \tag{2}$$

where $\psi_i = (c_{i\uparrow},c_{i\downarrow})^T$ and $c_{i\uparrow}$ $(c_{i\downarrow})$ is the annihilation operator on site i with spin $\uparrow$ $(\downarrow)$. σ_0 and $\sigma_{x,y,z}$ are the unit 2×2 matrix and the Pauli matrix for spin, a is the lattice length, and $\delta\hat{\mathbf{x}}$ $(\delta\hat{\mathbf{y}})$ is the unit vector along the x (y) direction. In our calculations, we set $A = B = 1$, the lattice length $a = 1$, and $\hbar = 1$.

In proximity to an s-wave superconductor, a finite pairing potential Δ can be induced in QAHI. This gives us the Bogoliubov–de Gennes (BdG) Hamiltonian

$$H_{\text{BdG}} = \frac{1}{2}\begin{pmatrix} H_{\text{QAHI}}(p) + \mu_S & i\Delta\sigma_y \\ -i\Delta^*\sigma_y & -H^*_{\text{QAHI}}(-p) - \mu_S \end{pmatrix}, \tag{3}$$

where μ_S is potential energy varied by the top-gated voltage and the basis vector is $(c_\uparrow(p),c_\downarrow(p),c_\uparrow^\dagger(-p),c_\downarrow^\dagger(p))^T$. For

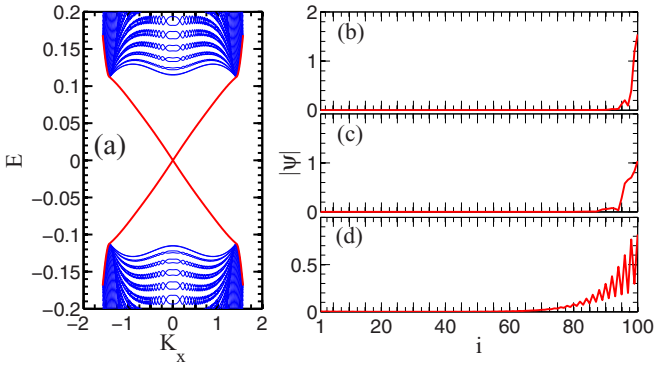

FIG. 2. (a) Band structure of TSC nanoribbon with $\mu_S = 1.5$ and (b)–(d) the wave functions Ψ_i of Majorana edge states versus the site i with the energy $E = 0$ for (b) $\mu_S = 0$, (c) $\mu_S = 0.6$, and (d) $\mu_S = 1.7$. The superconductor gap $\Delta = 0.35$, $m = -0.5$, and the ribbon width $N = 100a$.

$m < -(\Delta^2 + \mu_S{}^2)^{1/2}$, the TSC phase with $\mathcal{N} = 2$ is obtained, which owns two chiral Majorana modes [37]. Whereas the TSC phase with $\mathcal{N} = 1$ is realized by setting $-(\Delta^2 + \mu_S{}^2)^{1/2} < m < (\Delta^2 + \mu_S{}^2)^{1/2}$, which supports a single Majorana edge state propagating at the edges of the sample. To directly picture this edge state, we calculate the energy dispersion of the TSC phase with $\mathcal{N} = 1$ in Fig. 2(a). One can see that a pair of chiral gapless edge-state modes traverses across the bulk band gap. The corresponding wave functions Ψ_i of edge states are shown in Figs. 2(b)–2(d). One can see that the wave functions Ψ_i are completely localized at the system boundary for $\mu_S = 0.0$ and $\mu_S = 0.6$. However, wave functions Ψ_i oscillates and its localization length is considerably increased while $|m| \ll \mu_S$. The reason is that the system at $|m| \ll \mu_S$ is metal with a high density of states for $\Delta = 0$. For $m > (\Delta^2 + \mu_S{}^2)^{1/2}$, the system is in normal superconductor phase of $\mathcal{N} = 0$.

We now turn to analyze the scattering processes when an incident electron with the energy E flows from the left QAHI terminal into the central TSC region. By using the nonequilibrium Green's function technique [40], we can obtain the normal tunneling coefficient T, the LAR coefficient T_{LAR}, and the CAR coefficient T_{CAR} [41–43]:

$$T(E) = \text{Tr}\left[\Gamma^L_{ee} G^r_{ee} \Gamma^R_{ee} G^a_{ee}\right], \tag{4}$$

$$T_{\text{LAR}}(E) = \text{Tr}\left[\Gamma^L_{ee} G^r_{eh} \Gamma^L_{hh} G^a_{he}\right], \tag{5}$$

$$T_{\text{CAR}}(E) = \text{Tr}\left[\Gamma^L_{ee} G^r_{eh} \Gamma^R_{hh} G^a_{he}\right], \tag{6}$$

where e (h) represents electron (hole), respectively, and $\Gamma^L(E) = i[\Sigma^r_L - \Sigma^a_L]$ and $\Gamma^R(E) = i[\Sigma^r_R - \Sigma^a_R]$ are the linewidth functions. $G^r(E) = [E - H_{\text{BdG}} - \Sigma^r_L - \Sigma^r_R]^{-1}$ is the retarded Green's function, where H_{BdG} is the BdG Hamiltonian of the central TSC region. Σ^a_L, Σ^r_L, and Σ^r_R are the self-energies due to the coupling between the left (L) and right (R) QAHI leads and the central TSC region and can be numerically calculated [44].

III. NUMERICAL RESULTS AND ANALYSIS

In this section, we investigate the normal tunneling coefficient T, the LAR coefficient $T_{\rm LAR}$, and the CAR coefficient $T_{\rm CAR}$. Figure 3 shows these coefficients as a function of μ_S, where the energy $E = 0$ of the incident electron is fixed. From Fig. 3 one can see that, when μ_S is approximately less than 0.35, both the LAR coefficient $T_{\rm LAR}$ and the CAR coefficient $T_{\rm CAR}$ are zero and the normal tunneling coefficient T shows a quantized plateau with value of integer 1. The reason is that the TSC phase of $\mathcal{N} = 2$ is obtained by setting $m < -(\Delta^2 + {\mu_S}^2)^{1/2}$, in which there exist two branches of chiral Majorana edge states in the central region and the TSC is topologically equivalent to the QAHI with a single branch of the chiral fermion edge state. Thus the edge current is perfectly transmitted with the help of the edge states [37]. When the condition $m^2 < \Delta^2 + {\mu_S}^2$ is satisfied by increasing $\mu_S > (m^2 - \Delta^2)^{1/2}$, the TSC phase transits from $\mathcal{N} = 2$ to $\mathcal{N} = 1$ and there only exists a chiral Majorana state on the edges of the central region. Notice that the propagating directions of the chiral Majorana states for the QAHI-TSC interface and the vacuum-TSC interface are different. As shown in Fig. 1, at the QAHI-TSC interface, the Majorana edge states γ_1 and γ_3 propagate along the clockwise direction. Whereas at the vacuum-TSC interface, γ_2 and γ_4 are anticlockwise. In this case, the incident electron from the left terminal will be separated into two Majorana fermions at the QAHI-TSC interface, i.e., $a_1 = \frac{\sqrt{2}}{2}(\gamma_1 + i\gamma_2)$, thus γ_2 directly propagates to the right terminal and γ_1 returns back to the left terminal, i.e., $\gamma_1 \to \frac{\sqrt{2}}{2}(b_1 + b_1^\dagger)$ and $\gamma_2 \to \frac{\sqrt{2}}{2i}(b_2 - b_2^\dagger)$, where a_1 (a_2) is the incoming edge mode in the left (right) terminal and b_1 (b_2) is the outgoing edge mode in the left (right) terminal. So, the four scattering processes, LAR, T, CAR, and normal reflection have equal probability with value of 1/4 fraction [37], which can be clearly seen in Fig. 3 with $\mu_S \sim |m|$.

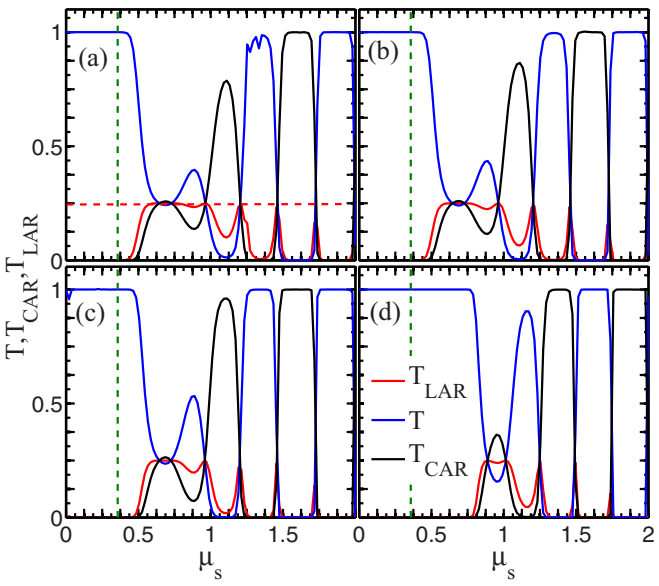

FIG. 3. The normal tunneling, LAR, and CAR coefficients as a function of top-gated voltage μ_S where $\Delta = 0.35$ and the energy $E = 0$ of the incident electron. $m = -0.5$, the length of the central TSC is $L = 20a$, and the ribbon width is (a) $N = 80a$, (b) $100a$, and (c) $150a$. In panel (d), $N = 100a$ and $m = -0.8$. The vertical dotted line in panels (a)–(d) is the boundary of the TSC phases with $\mathcal{N} = 2$ and $\mathcal{N} = 1$.

Most importantly, with increasing μ_S, one can see that normal tunneling and the CAR show oscillations as functions of μ_S and alternately display a quantum plateau with a value of integer 1 at $\mu_S > 1$. The plateau $T_{\rm CAR} = 1$ means the occurrence of the perfect CAR, and all other processes, the normal tunneling, LAR, and normal reflection are totally suppressed. Thus an electron incoming from the left terminal is completely transformed into a hole outgoing to the right terminal. In addition this perfect CAR is independent of the ribbon width as shown in Figs. 3(a)–3(c), where the width of sample varies from $80a$ to $150a$.

The reason behind this observation is that there exists the tunneling between Majorana edge modes γ_1 and γ_3 at certain system lengths. Thus the outgoing Majorana state $\frac{\sqrt{2}}{2}(b_1 + b_1^\dagger)$ in the left terminal can be written as

$$(\sqrt{2}/2)(b_1 + b_1^\dagger) = r\gamma_1 + te^{i\varphi}\gamma_3, \tag{7}$$

where $te^{i\varphi}$ is the tunneling amplitude between γ_1 to γ_3 satisfying $r^2 + t^2 = 1$. Notice that the phase φ can only take the value 0 or π because the Majorana fermion is a self-Hermitian particle. Similarly, the other three outgoing Majorana edge states are

$$(\sqrt{2}/2i)(b_1 - b_1^\dagger) = \gamma_4, \tag{8}$$

$$(\sqrt{2}/2)(b_2 + b_2^\dagger) = r\gamma_3 + te^{i\varphi}\gamma_1, \tag{9}$$

$$(\sqrt{2}/2i)(b_2 - b_2^\dagger) = \gamma_2. \tag{10}$$

This gives a scattering matrix

$$\begin{pmatrix} b_1 \\ b_1^\dagger \\ b_2 \\ b_2^\dagger \end{pmatrix} = \frac{1}{2}\begin{pmatrix} r & r & t_+ & t_- \\ r & r & t_- & t_+ \\ t_+ & t_- & r & r \\ t_- & t_+ & r & r \end{pmatrix}\begin{pmatrix} a_1 \\ a_1^\dagger \\ a_2 \\ a_2^\dagger \end{pmatrix}, \tag{11}$$

where $t_\pm = te^{i\varphi} \pm 1$. So the normal reflection coefficient $R = \frac{r^2}{4} = \frac{1-t^2}{4}$, the LAR coefficient $T_{\rm LAR} = \frac{r^2}{4} = \frac{1-t^2}{4}$, the normal tunneling coefficient $T = |t_+|^2/4$ and the CAR coefficient $T_{\rm CAR} = |t_-|^2/4$.

The results of Fig. 3 can be further illustrated as follows: For $\mu_S \sim |m|$, the Majorana edge state is localized at the boundary of the sample [see Fig. 2(b)], in this case the tunneling amplitude t between γ_1 and γ_3 is almost zero, which leads to $T = R = T_{\rm LAR} = T_{\rm CAR} = 1/4$. Whereas the wave functions of Majorana edge state Ψ_i oscillates and its localization length is considerably increased for $\mu_S \gg |m|$ [see Figs. 2(b)–2(d)]. Thus for a short central TSC region, it is inevitable that γ_1 could arrive at the right terminal by tunneling itself to γ_3 and the tunneling amplitude t can almost be 1. In this case, the normal reflection and LAR are completely suppressed, and the normal tunneling or CAR coefficient is 1, which can be clearly seen in Fig. 3. To be specific, in Fig. 1(b) we show the propagating route of the carriers. When an electron a_1 incoming from the left terminal spreads to the interface between QAHI and TSC, it will separate into two Majorana fermions γ_1 and γ_2. Here

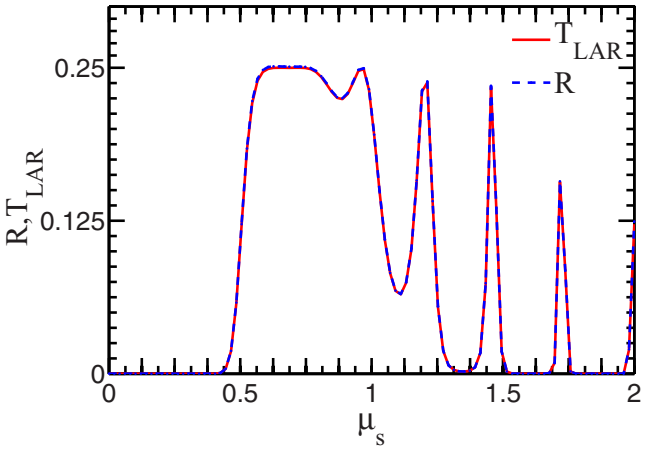

FIG. 4. The normal reflection coefficient R and the LAR coefficient $T_{\rm LAR}$ as a function of μ_S. The parameters are the same as those in Fig. 3(b).

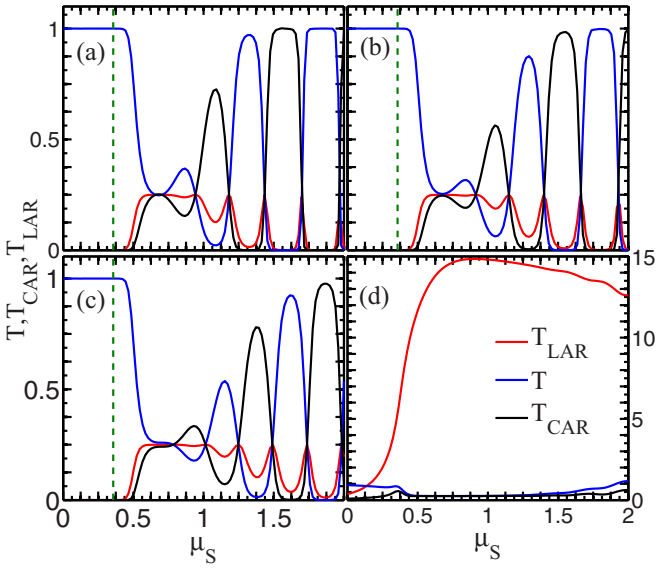

FIG. 5. T, $T_{\rm LAR}$, and $T_{\rm CAR}$ as a function of μ_S with (a) $\mu_L = 0.1$, (b) 0.2, (c) 0.4, and (d) 0.6. Other parameters are the same as those in Fig. 3(b). The vertical dotted line in panels (a)–(c) is the boundary of the TSC phases with $\mathcal{N} = 2$ and $\mathcal{N} = 1$.

γ_2 directly propagates to the right terminal, and γ_1 propagates along the interface between QAHI and TSC. If the quantum tunneling does not take place between the Majorana edge states γ_1 and γ_3, γ_1 will be reflected back to the left terminal once it arrives at the upper edge of the sample. In fact, for a short central TSC region, it is inevitable that γ_1 could arrive at the right terminal by tunneling it to γ_3. Therefore the outgoing states in the right terminal are γ_2 and $e^{i\varphi}\gamma_1$. Note that here φ can only be 0 or π due to the Majorana fermion being a self-Hermitian particle. For $\varphi = 0$, the normal tunneling coefficient T is 1 and the CAR coefficient $T_{\rm CAR}$ is 0. In contrast, for $\varphi = \pi$, the normal tunneling coefficient T is 0 and the CAR coefficient $T_{\rm CAR}$ is 1, i.e., the perfect CAR occurs and all other processes (T, LAR, and R) are totally suppressed. Here we would like to emphasize that φ can only be 0 or π is a decisive factor for the appearance of the plateaus of $T_{\rm CAR}$ and T.

In addition, from Eq. (11), we can see that the normal reflection and LAR coefficients are always equal ($R = T_{\rm LAR} = \frac{1-t^2}{4}$) regardless of the system parameters and $te^{i\varphi}$, which is also shown in the results of numerical calculations in Fig. 4. One can see that the normal reflection and LAR coefficients are exactly the same, although both R and $T_{\rm LAR}$ change complicatedly with the increase of μ_S. This is completely consistent with the Eq. (11) and clearly indicates why the physical picture for the quantum perfect CAR is reasonable. It is noteworthy that the TSC phase is $\mathcal{N} = 2$ whenever the μ_S satisfies $m < -(\Delta^2 + \mu_S^2)^{1/2}$. In this case, the normal tunneling coefficient T always is 1, so R and $T_{\rm LAR}$ still remain equal to 0.

Next we investigate how the perfect CAR is affected by the systemic parameters. Figures 3(a)–3(c) show the normal tunneling coefficient T, the LAR coefficient $T_{\rm LAR}$, and the CAR coefficient $T_{\rm CAR}$ for the different width N. It can be clearly seen that the CAR plateau with $T_{\rm CAR} = 1$ can well keep with the change of width except for the very narrow case. While the width is very narrow, there is the coupling between the upper and lower Majorana edge states, which can reduce $T_{\rm CAR}$. In addition, the perfect CAR can well survive with the change of the parameter m [see Fig. 3(d)].

Figure 5 shows the normal tunneling coefficient T, the CAR coefficient $T_{\rm CAR}$, and the LAR coefficient $T_{\rm LAR}$ versus the potential energy μ_S for the different on-site energy μ_L of the QAHI leads. The CAR plateaus with $T_{\rm CAR} = 1$ can well hold at the small μ_L as shown in Figs. 5(a)–5(b). For a large μ_L, the Fermi level is close to the bulk states, which could trigger the LAR and normal reflection and weaken normal tunneling and the CAR. In this case, T and the CAR show peaks with the values less than 1 [see Fig. 5(c) with $\mu_L = 0.4$]. Finally, for a very large μ_L, the Fermi level is in the bulk states of the QAHI, leading to an anomalous large LAR coefficient and the vanishing CAR as the general normal lead-superconductor system [see Fig. 5(d)].

Furthermore, Fig. 6 shows T, $T_{\rm CAR}$, and $T_{\rm LAR}$ for the different length L of the central TSC region. One can see that the plateaus of T and $T_{\rm CAR}$ are broken with the increase of distance between the two terminals. Even in this case, the larger μ_S is, the more robust is the plateau. For a long length L, the tunneling probability t between the Majorana edge states γ_1 and γ_3 is not equal to 1, thus both T and $T_{\rm CAR}$ are not also quantized. As the increasing L reaches a limit value, t tends towards zero and the four coefficients tend towards $T = R = T_{\rm LAR} = T_{\rm CAR} = 1/4$.

In Fig. 7 we plot T, $T_{\rm LAR}$, and $T_{\rm CAR}$ as functions of the superconductor pairing potential Δ at the different potential energy μ_S. For the small μ_S, the normal tunneling shows a quantized plateau with value of integer 1 and the other three coefficients (R, $T_{\rm LAR}$, and $T_{\rm CAR}$) are zero [see Fig. 7(a)]. The reason is that the central region is in the TSC phase of $\mathcal{N} = 2$ when the condition $m < -(\Delta^2 + \mu_S^2)^{1/2}$ is satisfied. Whereas for $m^2 < \Delta^2 + \mu_S^2$, the central region is in the TSC phase of $\mathcal{N} = 1$. Now the perfect CAR with $T_{\rm CAR} = 1$ can occur and all other scattering processes are totally suppressed [see Figs. 7(b) and 7(d)]. Thus the perfect CAR can exist in a wide range of Δ. And the larger μ_S is, the wider is the plateau value of CAR

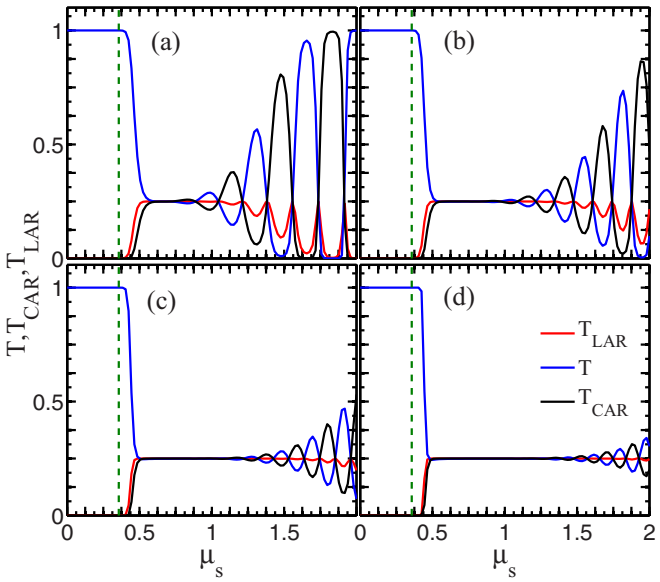

FIG. 6. T, $T_{\rm LAR}$, and $T_{\rm CAR}$ as a function of μ_S with the length of the central TSC region (a) $L = 30a$, (b) $40a$, (c) $50a$, and (d) $60a$. Other parameters are the same as those in Fig. 3(b).

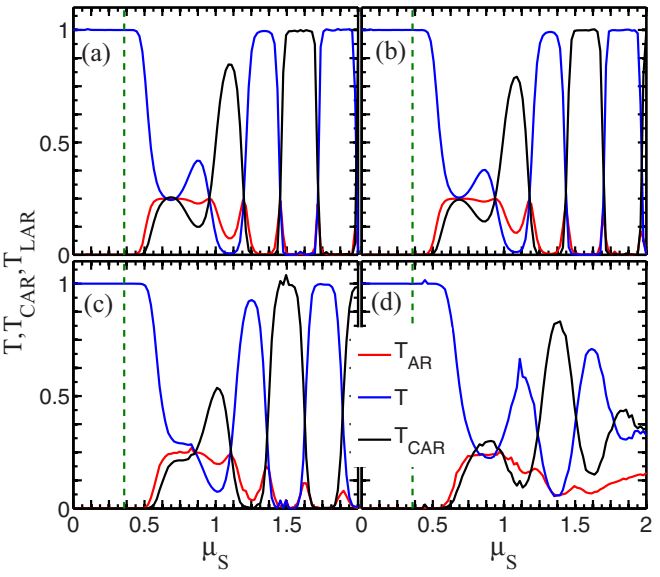

FIG. 8. T, $T_{\rm LAR}$, and $T_{\rm CAR}$ as a function of μ_S, with the disorder strengths being (a) $W = 0.5$, (b) 1.0, (c) 2.0, and (d) 3.0. Other parameters are the same as those in Fig. 3(b). Here the curves are averaged over 1000 random configurations.

coefficient. In addition, the quantized normal tunneling can also occur in $m^2 < \Delta^2 + \mu_S^2$ [see Fig. 7(c)] because of the alternate appearance of $T_{\rm CAR} = 1$ and $T = 1$ with the change of μ_S.

Next we consider the inevitable impurity scattering in the real samples. In Fig. 8 we consider the Anderson disorder only existing in the central TSC region. One can see that the perfect CAR plateaus are robust against the disorder and the plateaus can be well kept while the disorder strength is $W \lesssim 2$. In fact, the perfect CAR originates from the Majorana edge states. As soon as the ribbon is wide enough, the coupling between the upper and lower edge states is suppressed, then the perfect CAR always occurs. On the other hand, when the disorder becomes stronger (e.g., $W = 3.0$), the Majorana edge state as well as the TSC phase are destroyed because of the impurity scattering, then the quantized CAR plateau is destroyed and the CAR coefficient shows the peaks.

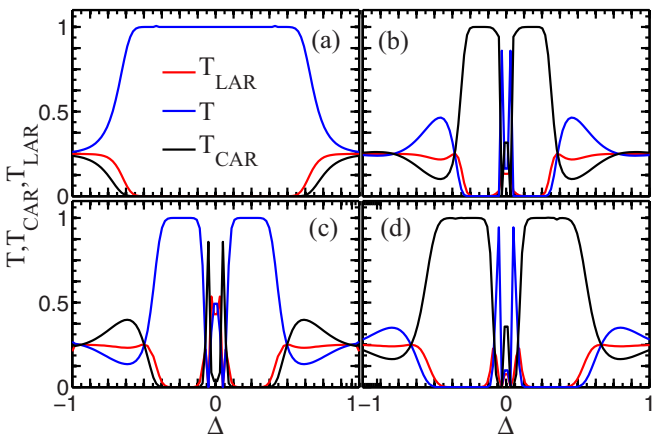

FIG. 7. T, $T_{\rm LAR}$, and $T_{\rm CAR}$ as a function of superconductor gap Δ with (a) $\mu_S = 0.2$, (b) 1.2, (c) 1.4, and (d) 1.6. Other parameters are the same as those in Fig. 3(b).

Up to now, we have demonstrated that a quantized perfect CAR occurs in the QAHI-$\mathcal{N} = 1$ TSC-QAHI system, in which two electrons from a Cooper pair at TSC are split and certainly go to two different leads. At last, we study the current in each terminal. By solving the transmission coefficients, the current I_L (I_R) from the left (right) QAHI terminal can be obtained straightforwardly [41,42] as

$$I_i = \frac{e}{\hbar}\int \frac{dE}{2\pi}[(f_{i+} - f_S)T_{iS} + (f_{i+} - f_{i-})T_{\rm LAR} + (f_{i+} - f_{\bar{i}-})T_{\rm CAR} + (f_{i+} - f_{\bar{i}+})T], \quad (12)$$

where $i = L$ (R) corresponds the left (right) terminal, $\bar{i} = R$ for $i = L$ whereas $\bar{i} = L$ for $i = R$, $f_{i\pm}(E) = 1/\{e^{[(E\mp V_i)/k_B\mathcal{T}]} + 1\}$, and $f_S(E) = 1/\{e^{E/k_B\mathcal{T}} + 1\}$ are the Fermi distribution with bias V_i and temperature $\mathcal{T}$. Here the bias of TSC terminal has been set to zero. While $|E| < \Delta$, the tunneling coefficient T_{iS} from the QAHI terminal to TSC is zero. By setting the right QAHI terminal as a voltage probes with $I_R = 0$, we have $V_R = -V_L$ and V_R/I_L tends infinity while the quantized perfect CAR occurs. On the other hand, we have $V_R = V_L$ when $T = 1$. Thus with the change of μ_S, the $T_{\rm CAR}$ and T alternately are 1 (see Figs. 3, 5, and 8), resulting in the alternating bias of the right terminal with values of V_L and $-V_L$.

IV. CONCLUSIONS

In summary, a quantized perfect crossed Andreev reflection is found in the QAHI-TSC-QAHI system when the TSC phase of $\mathcal{N} = 1$ is realized. The coefficient of the crossed Andreev reflection shows the plateaus with the value being integer 1, and all other scattering processes, the normal reflection, the normal tunneling, and the local Andreev reflection are completely

suppressed. The quantized perfect crossed Andreev reflection originates from the chiral Majorana edge states and the tunneling between them, and it is robust against the disorder and can work in wide range of system parameters.

ACKNOWLEDGMENTS

This work was supported by NBRP of China (2015CB921102) and NSF-China under Grants No. 11004046, No. 11474084, No. 11574007, and No. 11274364.

[1] R. Horodecki, P. Horodecki, M. Horodecki, and K. Horodecki, Rev. Mod. Phys. **81**, 865 (2009).
[2] K. Modi, A. Brodutch, H. Cable, T. Paterek, and V. Vedral, Rev. Mod. Phys. **84**, 1655 (2012).
[3] L. Aolita, F. de Melo, and L. Davidovich, Rep. Prog. Phys. **78**, 042001 (2015).
[4] A. Einstein, B. Podolsky, and N. Rosen, Phys. Rev. **47**, 777 (1935).
[5] M. D. Reid, P. D. Drummond, W. P. Bowen, E. G. Cavalcanti, P. K. Lam, H. A. Bachor, U. L. Andersen, and G. Leuchs, Rev. Mod. Phys. **81**, 1727 (2009).
[6] J. M. Byers and M. E. Flatté, Phys. Rev. Lett. **74**, 306 (1995).
[7] G. Deutscher and D. Feinberg, Appl. Phys. Lett. **76**, 487 (2000).
[8] G. Falci, D. Feinberg, and F. W. J. Hekking, Europhys. Lett. **54**, 255 (2001).
[9] P. Recher, E. V. Sukhorukov, and D. Loss, Phys. Rev. B **63**, 165314 (2001).
[10] J. Wang, L. Hao, and K. S. Chan, Phys. Rev. B **91**, 085415 (2015).
[11] D. Beckmann, H. B. Weber, and H. v. Löhneysen, Phys. Rev. Lett. **93**, 197003 (2004).
[12] S. Russo, M. Kroug, T. M. Klapwijk, and A. F. Morpurgo, Phys. Rev. Lett. **95**, 027002 (2005).
[13] M. A. Nielsen and I. L. Chuang, *Quantum Computation and Quantum Information* (Cambridge University Press, Cambridge, 2000).
[14] G. B. Lesovik, T. Martin, and G. Blatter, Eur. Phys. J. B **24**, 287 (2001).
[15] N. M. Chtchelkatchev, G. Blatter, G. B. Lesovik, and T. Martin, Phys. Rev. B **66**, 161320(R) (2002).
[16] K. V. Bayandin, G. B. Lesovik, and T. Martin, Phys. Rev. B **74**, 085326 (2006).
[17] J. Ulrich and F. Hassler, Phys. Rev. B **92**, 075443 (2015).
[18] P. Recher and D. Loss, Phys. Rev. Lett. **91**, 267003 (2003).
[19] L. Hofstetter, S. Csonka, J. Nygard, and C. Schonenberger, Nature (London) **461**, 960 (2009).
[20] L. Hofstetter, S. Csonka, A. Baumgartner, G. Fülöp, S. d'Hollosy, J. Nygård, and C. Schönenberger, Phys. Rev. Lett. **107**, 136801 (2011).
[21] G. Michalek, T. Domanski, B. R. Bulka, and K. I. Wysokinski, Sci. Rep. **5**, 14572 (2015).
[22] C. Bena, S. Vishveshwara, L. Balents, and M. P. A. Fisher, Phys. Rev. Lett. **89**, 037901 (2002).
[23] L. G. Herrmann, F. Portier, P. Roche, A. Levy Yeyati, T. Kontos, and C. Strunk, Phys. Rev. Lett. **104**, 026801 (2010).
[24] P. Recher and D. Loss, Phys. Rev. B **65**, 165327 (2002).
[25] J. Cayssol, Phys. Rev. Lett. **100**, 147001 (2008).
[26] J. Wang and S. Liu, Phys. Rev. B **85**, 035402 (2012).
[27] Z. Hou, Y. Xing, A.-M. Guo, and Q.-F. Sun, Phys. Rev. B **94**, 064516 (2016).
[28] J. Nilsson, A. R. Akhmerov, and C. W. J. Beenakker, Phys. Rev. Lett. **101**, 120403 (2008).
[29] A. F. Andreev, Sov. Phys. JETP **19**, 1228 (1964).
[30] R. W. Reinthaler, P. Recher, and E. M. Hankiewicz, Phys. Rev. Lett. **110**, 226802 (2013).
[31] C. X. Liu, S. C. Zhang, and X. L. Qi, Annu. Rev. Condens. Matter Phys. **7**, 301 (2016).
[32] R. Yu, W. Zhang, H. J. Zhang, S. C. Zhang, X. Dai, and Z. Fang, Science **329**, 61 (2010).
[33] X. L. Qi, T. L. Hughes, and S. C. Zhang, Phys. Rev. B **78**, 195424 (2008).
[34] C. Z. Chang, J. Zhang, X. Feng, J. Shen, Z. Zhang, M. Guo, K. Li, Y. Ou, P. Wei, L. L. Wang, Z. Q. Ji, Y. Feng, S. Ji, X. Chen, J. Jia, X. Dai, Z. Fang, S. C. Zhang, K. He, Y. Wang, L. Lu, X. C. Ma, and Q. K. Xue, Science **340**, 167 (2013).
[35] C. Z. Chang, W. Zhao, D. Y. Kim, H. Zhang, B. A. Assaf, D. Heiman, S.-C. Zhang, C. Liu, M. H. W. Chan, and J. S. Moodera, Nat. Mater. **14**, 473 (2015).
[36] X. L. Qi, T. L. Hughes, and S. C. Zhang, Phys. Rev. B **82**, 184516 (2010).
[37] S. B. Chung, X.-L. Qi, J. Maciejko, and S.-C. Zhang, Phys. Rev. B **83**, 100512 (2011).
[38] J. J. He, J. Wu, T.-P. Choy, X.-J. Liu, Y. Tanaka, and K. T. Law, Nat. Commun. **5**, 3232 (2014).
[39] Y.-T. Zhang, X. Deng, Q.-F. Sun, and Z. Qiao, Sci. Rep. **5**, 14892 (2015).
[40] *Electronic Transport in Mesoscopic Systems*, edited by S. Datta (Cambridge University Press, Cambridge, 1995).
[41] Q.-F. Sun and X. C. Xie, J. Phys.: Condens. Matter **21**, 344204 (2009).
[42] S.-G. Cheng, Y. Xing, J. Wang, and Q.-F. Sun, Phys. Rev. Lett. **103**, 167003 (2009).
[43] Q.-F. Sun, J. Wang, and T.-H. Lin, Phys. Rev. B **59**, 3831 (1999).
[44] D. H. Lee and J. D. Joannopoulos, Phys. Rev. B **23**, 4997 (1981).